

# Use of quasi-static nanoindentation data to obtain stress–strain characteristics for metallic materials

J. Dean, J.M. Wheeler, T.W. Clyne\*

*Department of Materials Science & Metallurgy, Cambridge University, Pembroke Street, Cambridge CB2 3QZ, UK*

Received 30 December 2009; received in revised form 17 February 2010; accepted 19 February 2010

Available online 19 March 2010

## Abstract

This paper concerns optimization of procedures and algorithms for extraction of stress–strain relationships from quasi-static nanoindentation experiments, using finite element method modelling. Several issues are highlighted, including the usefulness of incorporating residual indent shape in the comparisons, as well as load–displacement–time data, and the significance of creep and interfacial friction. The study is focused on extruded copper bar, using a spherical indenter and assuming transverse isotropy throughout. It is shown that, using the methodology presented here, experimental nanoindentation data could be used to estimate the yield stress and work-hardening rate, with good accuracy, i.e. the yield stress could have been obtained to a precision of about  $\pm 10\%$ , and the work-hardening rate to about  $\pm 25\%$ . Such inferred constitutive relations are more likely to be reliable if the comparisons are made in regimes within which creep does not significantly influence the behaviour, and in general the timescale of measurement is important.

© 2010 Acta Materialia Inc. Published by Elsevier Ltd. All rights reserved.

*Keywords:* Nanoindentation; Finite element analysis; Creep; Non-destructive testing

## 1. Introduction

Depth-sensing nanoindentation is commonly employed for material characterization. For instance, the Young's modulus can be determined from the unloading portion of the measured load–displacement curve, while hardness can be calculated from measured peak loads and residual indentation areas. Procedures have also been proposed for the extraction of strain-hardening exponents, fracture toughness values, viscoelastic properties and creep parameters, although most of these incorporate gross simplifications and are in general of doubtful reliability. It is of particular interest to obtain constitutive relations, i.e. stress–strain curves,  $\sigma = f(\varepsilon, \dot{\varepsilon}, T)$ . This represents a major challenge, since the stress and strain fields beneath an indent are relatively complex (even for simple-shaped indenters), and the raw data obtained (primarily load–dis-

placement plots) cannot readily be interpreted so as to reveal constitutive relations.

In view of the complexity of these stress and strain fields, it is clear that comprehensive analysis, almost certainly involving finite element method (FEM) modelling, is likely to be essential. FEM simulations [1,2] have demonstrated that it is possible, using pre-specified constitutive relations, to obtain predicted load–displacement curves that agree quite well with those obtained experimentally. Unfortunately, what might be termed the inverse problem – i.e. the inference of constitutive relations from observed behaviour during indentation – is much less tractable. The underlying factors responsible for this are:

- (i) the relatively low sensitivity of measurable behaviour (such as load–displacement plots) to the characteristics being sought;
- (ii) the fact that these characteristics incorporate several degrees of freedom (e.g. unknown values of yield stress and work-hardening rate as a function of strain

\* Corresponding author. Tel.: +44 1223 334332; fax: +44 1223 334567.  
E-mail address: [twc10@cam.ac.uk](mailto:twc10@cam.ac.uk) (T.W. Clyne).

and, in some cases, strain rate, plus the possibility of creep effects); and

- (iii) the relatively high sensitivity of measurable behaviour to extraneous factors, such as physical boundary conditions (e.g. frictional effects [3], surface layers, material anisotropy [4,5], tip shape imperfections [6], etc.).

While not expressed in quite these terms, the recent survey of Guelorget and Francois [7] highlighted this issue of sensitivity as being mainly responsible for the low accuracy and reliability of extracted constitutive relations obtained hitherto.

Nevertheless, there have been several recent studies [7–14] of the inverse problem, and in principle it is readily tackled, i.e. the input constitutive relations are adjusted until good agreement is found with experiment (commonly load–displacement curves). One issue is whether this adjustment process can be optimized in some way. Bouzakis and co-workers [9,10] presented their “Fast Approach of stress–strain curves based on nanoindentation” (FANOS) algorithm, which is designed to do this and is claimed to be efficient in terms of computing time. Lee et al. [11] suggested using numerical regression analysis, focusing on yield stress and a strain-hardening exponent as the key property parameters.

However, Dao et al. [8], and subsequently Pelletier [12], recognized the problem of sensitivities as being the underlying cause of poor reliability and accuracy. Pelletier focused on the role of indenter shape. Of course, one way of addressing the relatively low sensitivity of the experimental response to the constitutive relation is to broaden the range of experimentation, and carrying out tests on the same material with several different indenter shapes is clearly one possibility. This was in fact the approach adopted by Heinrich et al. [15] in their parametric FEM study. They concluded that using information obtained from two indenters led to more accurate estimates of the Young’s modulus, yield stress, and strain-hardening exponent. Pelletier also suggested that extending the comparisons to include predicted and measured residual indent shapes would boost the sensitivity and aid convergence to the optimal constitutive relation. In his study, two different uniaxial stress–strain relationships – (i) an elastic–plastic solid and (ii) an elastic–plastic linear strain-hardening solid – gave almost identical indentation load–displacement curves, while the residual indent shapes differed markedly (pile-up for case (i) and sink-in for case (ii)). This possibility was also noted earlier by Liu et al. [16].

Other workers [13,14] have focused on the most appropriate functional form for the constitutive equation. However, it is clear that such concerns do not address the underlying sources of error, although it is certainly worth noting that the operative deformation mechanisms, and their relation to postulated analytical equations, are of significance. For instance, in some cases the indent is confined to a single grain within a specimen, leading to anisotropy associated with slip system orientations [4,5,16,17]. As an example, microinden-

tation experiments performed on body-centred cubic (bcc) single crystals of W and Mo ((1 0 0), (0 1 1), and (1 1 1) faces) indicate that pile-up is sensitive to slip system orientation [18]. The same is true for face-centred cubic (fcc) crystals, although Lim and Chaudhri [19] noted that the indentation hardness values obtained from two grains of different orientation ((1 1 0), (1 1 1)) in a polycrystalline copper sample were very similar. Nevertheless, the effects of crystallographic orientation on indentation response (i.e. load–displacement curves and residual indent topography) have not yet been fully investigated, although the approach adopted by Liu et al. [17] appears promising. In their study, load–displacement and residual indent data were obtained for single crystal copper in three orientations ((1 0 0), (0 1 1), and (1 1 1) faces), using a spherical indenter. These measured data were compared to FEM predictions obtained using a large deformation crystal plasticity user subroutine, incorporating the geometry of crystallographic slip. Correlations were established between the anisotropic nature of the surface topographies and the operative, orientation-dependent slip systems.

Of course, constitutive relations obtained in this way relate to the single crystal (and its particular orientation) only. In practice, it is much more likely that constitutive relations will be required for polycrystals, and, indeed, factors related to the polycrystalline nature of the material, such as the grain size and the texture, will affect the constitutive relation. It is therefore clear that, in order to characterize the behaviour of polycrystalline materials in this way, regions must be indented which contain more than just one or two grains.

Creep and other time-dependent phenomena also commonly occur during indentation [20–26]. It is sometimes assumed that creep effects are negligible (at room temperature), but in practice they are often highly significant, at least for metals. Indentation tends to produce relatively high local stresses and it is fairly common experience for these to generate obvious time-dependent effects, such as progressive indenter penetration when a constant load is maintained. It therefore seems likely that, at least in many cases, it will be necessary to take account of the possibility of creep affecting the results when experimental nanoindentation data are to be used to obtain constitutive relations. Of course, it may also be possible to obtain creep parameters from nanoindentation data, although this presents major challenges and there has certainly been very little success in this area so far [23].

Finally, it is becoming clear that friction between indenter and specimen can affect the observed behaviour. The analyses of Mesarovic and Fleck [27] suggest that pile-up formation is likely to be inhibited by friction. The stress field beneath the indenter was also reported to be affected by friction. Mata and Alcalá [28] modelled the effect of the indenter–specimen friction coefficient on: (i) hardness, (ii) surface deformation (i.e. pile-up or sink-in) and (iii) load–displacement curve. They noted that friction was important for solids that would ordinarily exhibit pronounced pile-up

(i.e. those exhibiting low strain-hardening exponents, or low work-hardening rates), since it acted to oppose slippage at the interface. For solids that would ordinarily exhibit only moderate pile-up (or even sink-in), on the other hand, friction was less significant, since slippage at the interface would be limited in any event. In these cases, the load response and the plastic strain field remained relatively unaffected. However, the FEM simulations carried out by Antunes et al. [29], concerning Vickers indentation into AISI M2 steel (with a low strain-hardening exponent of 0.01), for three friction coefficient values, gave predicted load–displacement plots that were indistinguishable. This appears inconsistent with the above rationale, although it is possible that all of the coefficient values used were large enough to eliminate interfacial slippage. This is clearly an area requiring further study, particularly since there has been virtually no experimental work in which friction coefficients have been varied or measured.

In summary, while material constitutive relations can, in principle, be obtained using FEM modelling and experimental nanoindentation data, in reality it has proved difficult to employ such procedures with any confidence, since experimental data have tended to be relatively noisy and similar levels of agreement between prediction and experiment can often be obtained using a wide range of constitutive relations. Developing a more robust procedure requires two types of improvement: (i) broadening of the range of experimental data being used to obtain convergence to a unique solution and (ii) reducing the errors caused by inadequate capture of the effects contributing to the observed behaviour. This paper is aimed at making progress on both fronts.

## 2. Experimental procedures

### 2.1. Material

The experimental work in this study has been carried out using extruded OFHC copper bar in its as-received

form. Specimens for metallographic investigation were cut from the bar using electric discharge machining (EDM). Samples were mechanically polished using conventional procedures. The specimen surface was etched with dilute ferric chloride. A micrograph of a polished and etched surface is presented in Fig. 1a. It can be seen that a range of grain sizes is present. Some are larger than the diameter of the indenter tip used in the current work (nominally 20  $\mu\text{m}$ ), while some are smaller. In order to obtain a polycrystalline response, data from indents such as that shown in Fig. 1b have been studied, since it straddles several grains. It was noted that, when this was the case, reproducible load–displacement plots were obtained during indentation, whereas if smaller indents were produced (within single grains), then much greater variations were observed in the load–displacement plots (see Section 2.3 below).

### 2.2. Macroscopic mechanical testing

#### 2.2.1. Plastic deformation

Macroscopic mechanical properties were measured using conventional mechanical test procedures, focussing mainly on the extrusion direction, which was also the direction of indentation. Cylindrical specimens (6 mm diameter and 8 mm height) were tested in compression, using a 10 kN Instron hydraulic mechanical test machine, under displacement control, with a displacement rate of 0.001  $\text{mm s}^{-1}$  – i.e. an initial strain rate of  $2 \times 10^{-5} \text{ s}^{-1}$ . Compression tests were conducted along the extrusion axis. The specimens were located between flat platens of silicon carbide. The ends were lubricated with molybdenum disulphide, to minimize barrelling. Displacements were measured using an LVDT.

#### 2.2.2. Creep behaviour

Specimens for creep testing were CNC-machined from the copper rod, and loaded in uniaxial tension along the

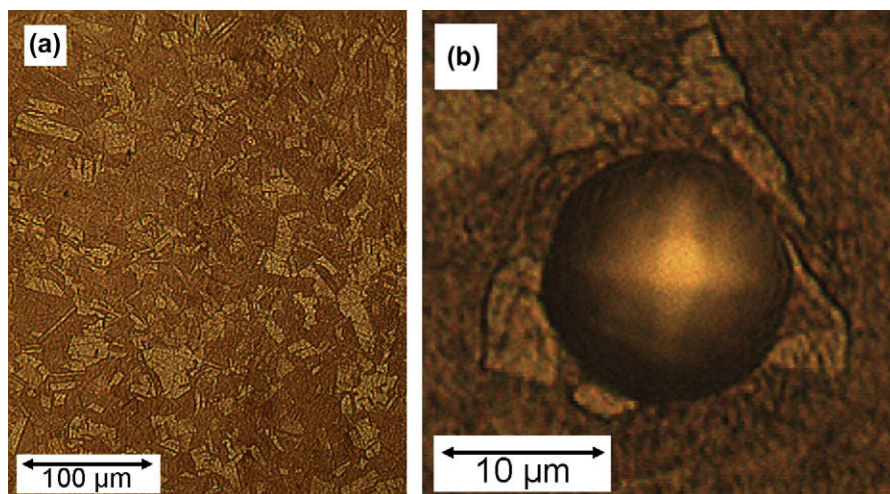


Fig. 1. Optical micrographs of the as-received copper, at: (a) low and (b) high magnifications, with the latter including an indent produced by a (nominally 10  $\mu\text{m}$  radius) spherical indenter loaded so as to penetrate to an initial depth of 1.65  $\mu\text{m}$ .

extrusion axis. Testing was carried out using a series of stresses and temperature ( $\sigma = 50, 150$  and  $250$  MPa, and  $T = 291, 373$  and  $473$  K), under load control (with a weight acting under gravity). Displacements were measured using clip gauges.

### 2.3. Indentation procedure

Indentation testing was carried out using a pendulum-based nanoindenter – the Nanotest 600, supplied by MicroMaterials Ltd. Tests were carried out using a spherical diamond indenter (nominally  $20\ \mu\text{m}$  diameter), with the indentation direction parallel to the extrusion axis of the copper bar. The testing was carried out under load control. All tests were carried out at ambient temperature ( $291\ \text{K} \pm 2\ \text{K}$ ). For most cases, the loading rate was fixed at  $10\ \text{mN s}^{-1}$ . This progressive increase in the load was arrested when a depth of  $1.65\ \mu\text{m}$  had been attained. The period required to reach this depth, for a given material, was therefore dependent on the material response. Once the specified penetration depth had been reached, the load at that point was held constant for a specified period – in the present case, this was  $50\ \text{s}$ . The introduction of such a (dwell) period is common practice, designed to help ensure that the unloading response is purely elastic (and can thus be used to measure the elastic modulus). Part-way through the subsequent unloading (also at  $10\ \text{mN s}^{-1}$ ), a further hold period of  $30\ \text{s}$  was introduced, in order to check for any thermal drift. Similar operations were also carried out using a slow loading rate ( $0.5\ \text{mN s}^{-1}$ ). The system compliance was established using high load indentations on three reference materials, namely single crystal tungsten, a tool steel and fused silica. Data are presented after correction for this compliance.

The effect of the indent being confined to a single grain, as opposed to straddling several grains, is illustrated in Fig. 2. The load–displacement plots in Fig. 2a correspond to 10 indents made with a penetration depth of  $0.4\ \mu\text{m}$ , giving an indent diameter of about  $5\ \mu\text{m}$ , each of which was located within a single grain. The 20 plots shown in Fig. 2b, on the other hand, were made to a depth of  $1.65\ \mu\text{m}$ , giving a diameter of about  $17\text{--}18\ \mu\text{m}$ , each of which straddled several grains. It can be seen that the single grain plots exhibit considerable scatter, arising from the effect of grain orientation, whereas those of multiple grain indents are much more reproducible. One of the plots in Fig. 2b, i.e. the one having a thicker (blue) line, corresponds to an indent which forms the basis of comparisons in the present paper. It should, however, be noted that, while the scatter is relatively small, and the chosen plot is a “representative” one, it would not be justifiable to make any deductions dependent to a precision much better than, say,  $\pm 5\%$  on the absolute values of load or displacement. This level of variability is probably inherent in the degree to which the response of a small volume can reflect that of the bulk, although there may be a dependence on the grain structure and texture.

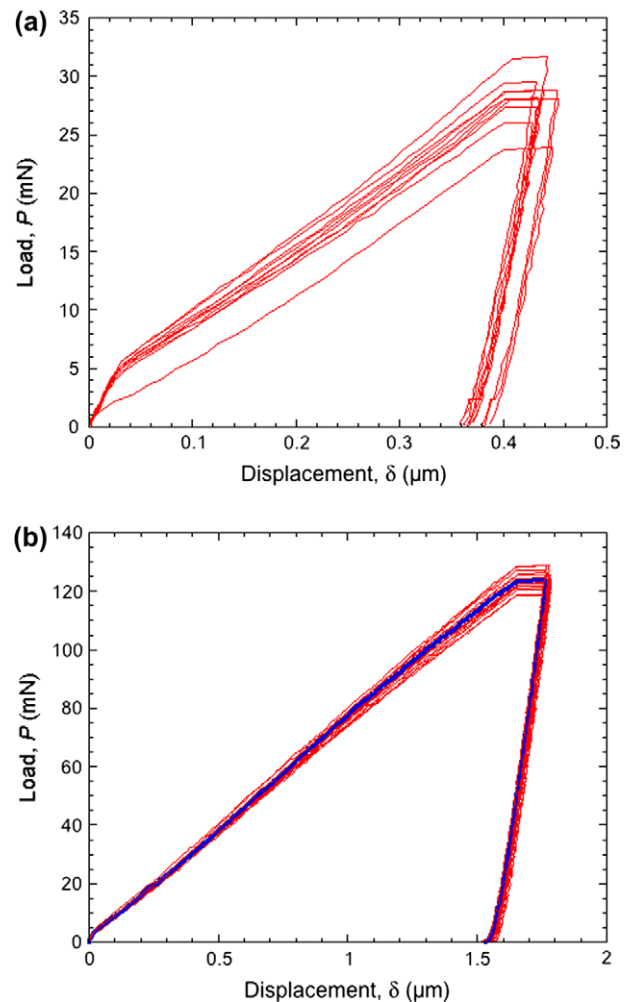


Fig. 2. Sets of load–displacement plots, obtained using an initial penetration depth of: (a)  $0.4\ \mu\text{m}$  and (b)  $1.65\ \mu\text{m}$ . In the first case, all of the indents were located within single grains, while in the second case they all straddled several grains. The plot with the thicker (blue) line in (b) corresponds to the indent used for several comparisons in the current paper between measured and predicted behaviour. (For interpretation of the references to colour in this figure legend, the reader is referred to the web version of this article.)

The thermal drift rate was systematically monitored for the 20 indents represented in Fig. 2b. The average rate was about  $0.045\ \text{nm s}^{-1}$ . This is clearly a relatively low rate since, over the period of a typical test, it would aggregate up to just a few nm. This is certainly resolvable, but none of the deductions being made in the current work actually depends on resolutions of this order. Of course, if the drift can be assumed to be linear during the test period, then appropriate compensation can be made.

### 2.4. AFM measurements on indenter tip and residual indents

The indenter tip was characterized using a Veeco Dimension 3100 AFM system, with an XY closed-loop scanner using TappingMode™ with RTESPs (rotated tapping etched silicon probes). After locating the surface and apex of the indenter tip,  $512 \times 512$  pixel scans of  $15\ \mu\text{m}$

by 15  $\mu\text{m}$  were performed. Projected area functions were extracted from the data, using height histograms. The residual indent shapes were also characterized using the Veeco Dimension 3100 AFM system. After locating an indent, a 40  $\mu\text{m}$  by 40  $\mu\text{m}$  scan was taken. Analysis of the data was carried out using WsXM software from Nanotec [30].

### 3. FEM model formulation

#### 3.1. Meshing of the specimen and mechanical boundary conditions

An axi-symmetric model was employed in ABAQUS/CAE. In fact, even if the indenter itself is a perfect sphere, which is not usually the case, such indents do commonly exhibit at least some asymmetry, even when indenting polycrystals. However, the error introduced by this is thought to be small in the current work. The implicit solver was used for all simulations. The specimen was modelled as a deformable body and meshed with 5625 linear quadrilateral (hybrid) elements (type CAX4H). The hybrid element formulation is recommended [31] for incompressible materials and for cases when deformation is dominated by plastic flow. The mesh, which is shown in Fig. 3, was refined directly beneath the indenter, in order to improve the resolution in this region. A sensitivity analysis confirmed that this mesh was sufficiently fine to achieve convergence, numerical stability and mesh-independent results.

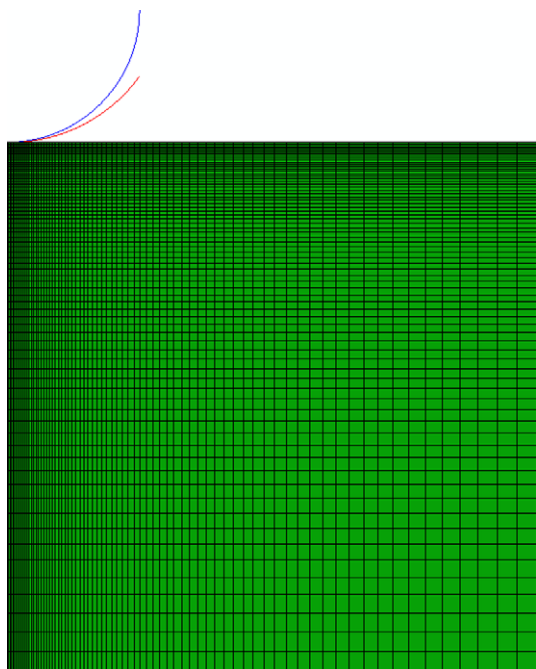


Fig. 3. The (axi-symmetric) FEM mesh employed in the model: also shown are a 10  $\mu\text{m}$  radius sphere (blue, upper curve) and an indenter section obtained from AFM measurements (red, lower curve). (For interpretation of the references to colour in this figure legend, the reader is referred to the web version of this article.)

It is common practice to model the indenter as an analytical rigid body of perfect sphericity. However, it should be noted that it is possible for the shape of such tips to deviate significantly from that of a perfect sphere. For instance, local defects may be present as well as systematic shape anisotropy (which can arise during machining from hardness differences in different crystallographic directions). Local defects probably just introduce a small level of noise into the measurements – this was the conclusion of Chen and Chang [6] – but systematic distortions of crystallographic origin may be worth noting. Of course, they are difficult to predict, but it may in some cases be justifiable to carry out topographic profiling of the tip and incorporate this measured shape into the FEM model. In the simulations presented here, however, the indenter was modelled as an analytical rigid body, with dimensions consistent with the AFM-determined area function (Section 2.4). This is often a worthwhile exercise, and in the present case it turned out that the AFM-determined shape differed significantly from that of an ideal 10  $\mu\text{m}$  radius sphere. This is apparent in Fig. 3, in which the AFM-determined shape is compared to that of the ideal sphere.

It is also important to consider carefully how the experimental conditions are being controlled during indentation, since precision is needed, not only in the acquisition of experimental data, but also in the way that the model is formulated. In the present case, the indenter load history (measured experimentally) was specified as a model boundary condition. In fact, it is probably more common for the maximum indenter displacement to be specified. In that case, the indenter load history can be predicted, for a given constitutive relation, and compared with the experimental data. In the present case, however, since the (measured) load history has been specified as input data for the model, a comparison between measured and predicted displacement–time curves is more meaningful, since both are effectively outcomes of an “experiment” (practical or modelling).

#### 3.2. Constitutive relations for material plasticity

It was assumed in the present work that the material exhibited linear work-hardening (see Section 4.1). This type of behaviour can be represented by an equation of the form

$$\sigma = \sigma_Y + K\varepsilon_p \quad (1)$$

where  $\sigma$  is the stress,  $\sigma_Y$  is the yield stress,  $\varepsilon_p$  is the equivalent plastic strain and  $K$  is the work-hardening rate. In order to explore the sensitivity of predicted behaviour to the work-hardening rate  $K$ , and the yield stress  $\sigma_Y$ , five linear constitutive relations have been employed.

#### 3.3. Simulation of creep deformation

ABAQUS provides a general framework for defining time-dependent viscoplastic behaviour via the user subroutine CREEP. This is based on the standard steady state creep rate equation

$$\frac{d\varepsilon}{dt} = A\sigma^n \exp\left(\frac{-Q}{RT}\right) \quad (2)$$

in which  $A$  is a constant,  $n$  is the stress exponent and  $Q$  is the activation energy. Increments of creep strain, in a given time increment, were calculated using this expression, taking no account of the prior strain history of the volume element concerned. Values of  $n$ ,  $A$  and  $Q$  were estimated from experimental data obtained during the macroscopic creep tests (Section 2.2.2). The simulations were thus based on the assumption that only steady state creep is exhibited, and that, if a change in stress level (or temperature) occurs in a particular region, it immediately deforms at the (steady state) rate corresponding to these new conditions, with no dependence on prior deformation history. As has been highlighted by Goodall and Clyne [23], such neglect of primary creep, and indeed of any prior strain history effects, may introduce substantial errors during simulation of indentation.

### 3.4. Simulation of friction between indenter and specimen

The effect of friction on the indentation response was investigated by incorporating a friction coefficient (independent of slippage rate and temperature) into the FEM model. This introduces a shear force opposing interfacial sliding, given by the product of the normal force and the friction coefficient. (Unless otherwise stated, the value of the friction coefficient was zero, i.e. friction was neglected.)

## 4. Experimental data, model predictions and sensitivity analysis

### 4.1. Macroscopic plasticity

An experimental stress–strain curve, obtained during compressive loading in the axial (extrusion) direction, is shown in Fig. 4. It can be seen that the yield stress is about

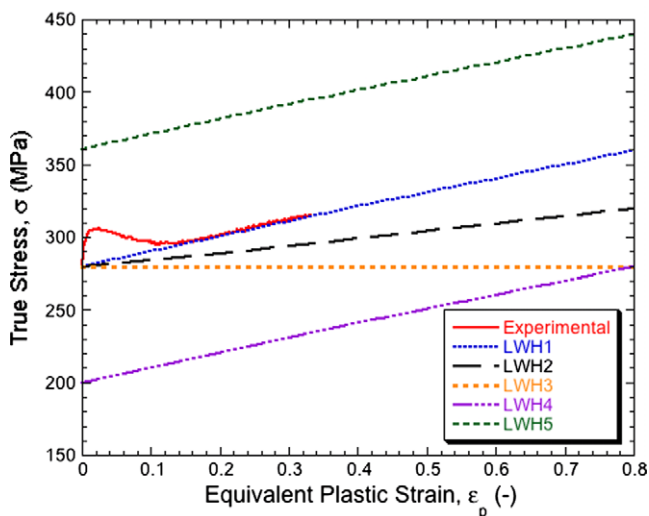


Fig. 4. Experimental stress–strain data for axial compression, together with the five different constitutive relations used in the FEM model.

280 MPa and, after an initial transient, the work-hardening rate is linear, at  $\sim 100$  MPa. Also shown in this figure are plots corresponding to five different constitutive relations, all with linear work-hardening rates. Relations LWH1–3 are based on a yield stress of 280 MPa, with work-hardening rates of 100, 50 and 0 MPa, respectively, while LWH4 and LWH5 are both based on work-hardening rates of 100 MPa, with yield stresses of 200 and 360 MPa, respectively. It can be seen that the LWH1 relation was designed to represent the observed experimental behaviour.

### 4.2. Creep deformation

Experimental (steady state) strain rate data are plotted in Fig. 5a, as a function of stress, together with curves obtained using Eq. (2), for the three temperatures concerned. These curves correspond to the (best fit) values of  $A$ ,  $n$  and  $Q$  shown in the figure. It is difficult to compare these values with expectations for copper, since creep behaviour is often quite sensitive to microstructure, and in any event there is little information in the literature for

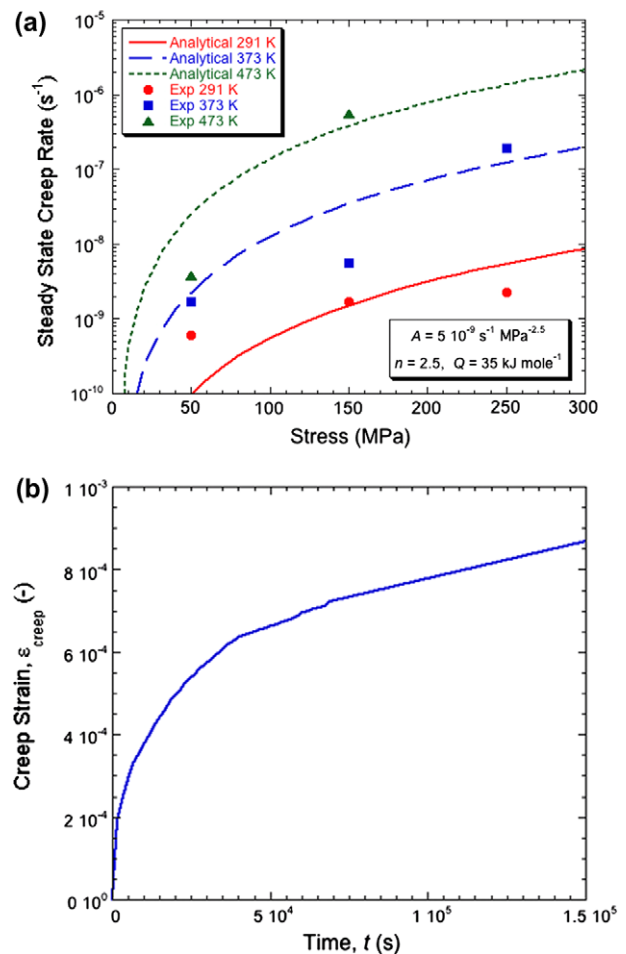


Fig. 5. Experimental creep data, showing: (a) steady state creep rates, as a function of applied stress and temperature, together with predictions from Eq. (2), obtained using the values of the creep parameters shown and (b) a creep strain history, for an applied stress of 250 MPa at room temperature.

the creep of copper over this temperature range. The value of  $Q$  ( $35 \text{ kJ mol}^{-1}$ ) is well below the activation energy for (lattice) diffusion in copper, but at these relatively low temperatures it is likely that fast diffusion paths, with lower activation energies, would predominate in the rate-determining processes.

In general, these values are plausible, and give fairly good agreement with the experimental data. Of course, they relate only to steady state behaviour, and give little or no information about the primary creep characteristics. As expected, there is a substantial variation in creep rate during the period prior to establishment of a steady state. This is illustrated by the creep strain plot shown in Fig. 5b, which refers to room temperature and an applied stress of 250 MPa. It may be noted that this plot is particularly relevant to the indentation experiments carried out in the present work, which were all done at room temperature and generated local stress levels of approximately this magnitude (i.e. around the yield stress) in significant volumes throughout the tests. The substantial difference between creep rates in primary and secondary (steady state) regimes can be noted by comparing initial and final gradients. For example, in a period of 100 s, a strain of about  $10 \mu\text{strain}$  would occur in the primary regime, while in the secondary regime only about  $0.1 \mu\text{strain}$  would result. This factor of 100 between these creep rates is obviously likely to result in large underestimates of the creep during indentation, if steady state rates are employed. Of course, in reality any particular volume element is likely to be in a condition corresponding to some intermediate point along the curve and the situation is further complicated by the fact that the stress in the element may be changing throughout the process. Nevertheless, the possibility that use of steady state creep rate data may give rise to substantial underestimates of the creep strain should be borne in mind.

### 4.3. Indentation

#### 4.3.1. Experimental data

During indentation, load–displacement–time data were continuously recorded. Typical data are presented in Fig. 6, which shows load and displacement histories for two different loading rates. The load history was in effect pre-specified (although the peak load was dependent on how the material deformed), while the response of the material is reflected in the displacement history. It is clear from this figure that time-dependent deformation (i.e. creep) is influencing the observed behaviour, at least for the lower loading rate, since the peak load (needed to create the specified indentation depth of  $1.65 \mu\text{m}$ ) is about 13% lower in that case. It follows that a significant proportion of the deformation that has occurred at the lower loading rate has taken place via creep mechanisms. This highlights the fact that, even at room temperature, it may be necessary to incorporate creep effects into this type of

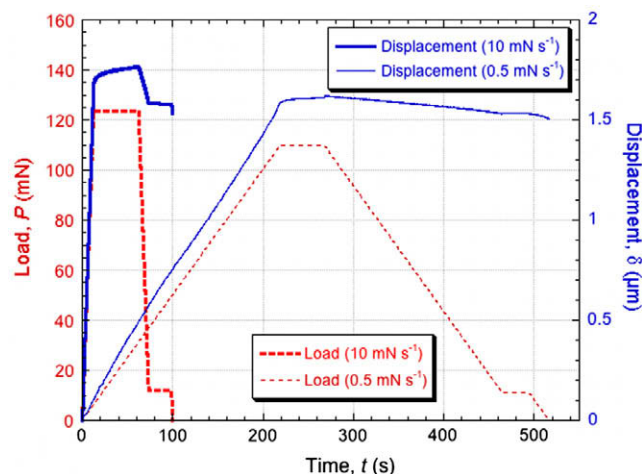


Fig. 6. Experimental data for load and displacement histories during indentation with two different loading rates. In both cases, a dwell period was introduced at the peak load and at a lower load.

modelling, at least for many materials (metals) and loading conditions.

#### 4.3.2. Predicted displacement histories

Predicted displacement–time plots, obtained using different constitutive relations, are compared with experimental data in Fig. 7, for high and low loading rates. There are several noteworthy features. Consider first the high loading rate case (Fig. 7a). The gradient ( $d\delta/dt$ ) during loading is predicted to exhibit some sensitivity to the work-hardening rate (compare LWH1–3), although the differences are small considering that the value is being varied from 0 (LWH3) to 100 MPa (LWH1). This gradient is more sensitive to the yield stress (compare LWH1, LWH4 and LWH5). However, the differences between the predictions are greater in terms of the displacement depth at the end of the loading period, or, equivalently, the load needed to reach a specified depth. It is clear that LWH1, which is the one designed to represent the macroscopically measured behaviour, gives good agreement in terms of the load (i.e. the time) needed to generate the specified displacement of  $1.65 \mu\text{m}$ . It would certainly have been picked in preference to LWH4 and LWH5, on the basis of this plot, i.e. the yield stress could have been established fairly accurately in this way. The outcome is less sensitive to the work-hardening rate, which is unsurprising in view of the fact that only a relatively small volume of specimen is experiencing large plastic strains. Nevertheless, the LWH1 prediction appears to be somewhat closer to the experimental plot than LWH2 or LWH3, although the caveat in Section 2.3 about there being something like a  $\pm 5\%$  uncertainty in the experimental data (load, or time, in this case) should be noted.

However, it can also be seen in Fig. 7a that the creep contribution to the behaviour during the dwell is not being well-captured – for example, the progressive penetration

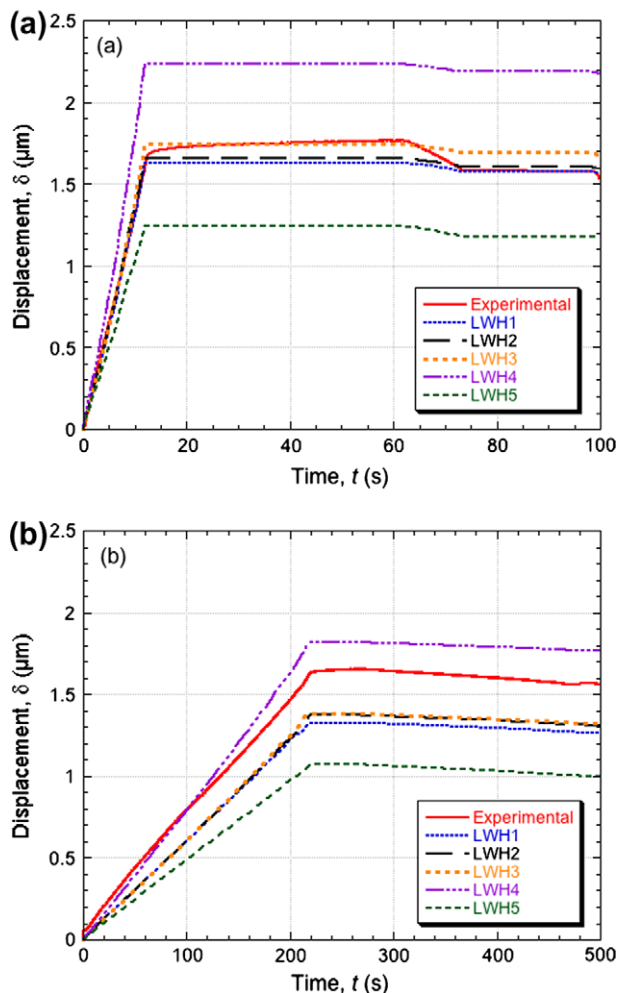


Fig. 7. Comparison between experimental displacement history data and predictions from the FEM model, for loading rates of: (a)  $10 \text{ mN s}^{-1}$  and (b)  $0.5 \text{ mN s}^{-1}$  (see Fig. 6), obtained using the creep parameters in Fig. 5 and the constitutive relations shown in the legend.

during the hold and the relaxation during the subsequent unloading period are both under-predicted. In fact, the overall contribution of creep to the behaviour is relatively small for this high loading rate case, particularly during the loading phase, and this facilitates accurate evaluation of the constitutive relation. However, this is not the case for the low loading rate experiment (see Fig. 7b). Creep is now making a major contribution to the behaviour, even during the loading phase, as was evident from the lower load needed to generate the specified displacement (Fig. 6). That this creep contribution to the behaviour is being under-predicted by use of the steady state expression (Eq. (2)), using the parameters shown in Fig. 5a, is now very clear, since the LWH1 plot gives substantially lower predicted penetration depths than actually occurred during these experiments. If this comparison had been used to infer the constitutive relation, then relatively large errors would probably have arisen, with the under-predicted creep deformation probably leading to anomalously low values being inferred for the yield stress and the work-hardening rate.

The reason for the creep deformation being under-predicted is not entirely clear. However, the most likely explanation lies in the neglect of primary creep. The assumption that the creep rate within any volume element instantaneously conforms to the steady state value for the stress level concerned, while mathematically tractable in a model of this type, is clearly unrealistic. In reality, primary creep behaviour, with creep rates substantially greater than those for the corresponding steady state, may strongly affect, and even dominate, the overall behaviour. This would be consistent with the suggestion of Goodall and Clyne [23]. If so, deduction of (steady state) creep rate parameters from indentation data will, to say the least, require some very careful measurement and analysis. Even taking account of the effect of creep for the purposes of inferring constitutive relations may require information about primary creep behaviour, rather than just steady state parameters. Of course, the obvious approach to this problem is to use indentation data obtained in regimes in which creep (steady state or primary) is not strongly influencing the observed behaviour, although careful modelling and measurement may be needed in order to identify these regimes with confidence.

#### 4.3.3. Residual indent shape

A comparison is shown in Fig. 8 between predicted and measured residual indent shapes, for the high loading rate case. The experimental plot represents a radial average of AFM data. As with the predicted displacement histories, certain features are particularly sensitive to the constitutive relations. In this case, the pile-up around the periphery of the indent is predicted to be greater when the material exhibits less work-hardening and/or has a lower yield stress. The predicted shape of the interior of the indent is also sensitive to the work-hardening rate, with a higher value giving shallower indents. The same is true of the yield stress. It can be seen that the sensitivity of the indent shape to yield stress and work-hardening rate is slightly different from that of the load–displacement response, and this may be helpful in attempting to converge on the “correct” constitutive relation. Of course, there are other, complementary approaches to making the procedures more discriminatory, such as using a range of tip shapes.

It can be seen in Fig. 8 that, of the constitutive relations employed, the “correct” one (LWH1) gives the closest agreement with the experimentally measured indent shape. Taken in conjunction with the corresponding displacement history comparison shown in Fig. 7a, which was not strongly affected by creep (at least during the loading phase), it is clear that the experimental indentation data, viewed in the light of FEM model predictions, can in this case be used to obtain a good estimate of the (correct) constitutive relation, at least if the assumption is made that the material exhibits linear work-hardening. This is clearly very encouraging, although it may be noted that, in addition to creep, there are other possible effects that might need to be taken into account, notably friction between indenter and specimen (see Section 4.3.4).

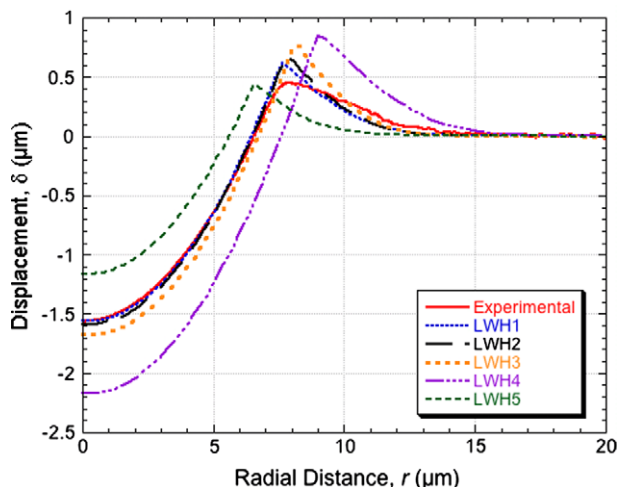


Fig. 8. Comparison between experimental residual indent shape data, for a loading rate of  $10 \text{ mN s}^{-1}$  (Fig. 6), and predictions from the FEM model, obtained using the creep parameters shown in Fig. 4 and the constitutive relations shown in the legend.

#### 4.3.4. Effect of friction

A comparison is shown in Fig. 9 between the measured displacement history and residual indent shape and the corresponding predictions, based on use of the LWH1 constitutive relation in conjunction with three different coefficients of friction. The “correct” value of the latter is not really known, although it probably lies in the range covered by these simulations. It can be seen that relatively small changes in the value of the coefficient, within this range, can have a significant effect on both displacement history and indent shape. Ideally, therefore, it should be measured for the case concerned, or at least a value should be employed which was obtained experimentally under similar conditions. Unfortunately, there are virtually no such data available at present. However, the sensitivity of the predictions to the value of the friction coefficient is not very high, and the predictions obtained using a value of zero actually seem to be closer than those for finite values, so the issue does not appear to be of major concern. Of course, one should again note that the experimental data acquired during the test (time, or load, in the case of Fig. 9a) carry an uncertainty of  $\pm 5\%$  just in terms of reproducibility. In any event, it would be very helpful if some experimental measurements of the friction coefficient could be made, although evidently this is quite a challenging objective.

#### 4.3.5. Stress and strain fields

Fig. 10a shows that, for the reference model case, predicted plastic strains after indentation range up to about 90%, with significant residual strains extending a micron or two below the indenter. Predicted contours of von Mises stress, at peak load and after the indenter has been retracted, are shown in Fig. 10b and c. Under peak load, the stress field extends to a depth of about  $20 \mu\text{m}$ , with peak stresses of about 350 MPa, while residual stresses

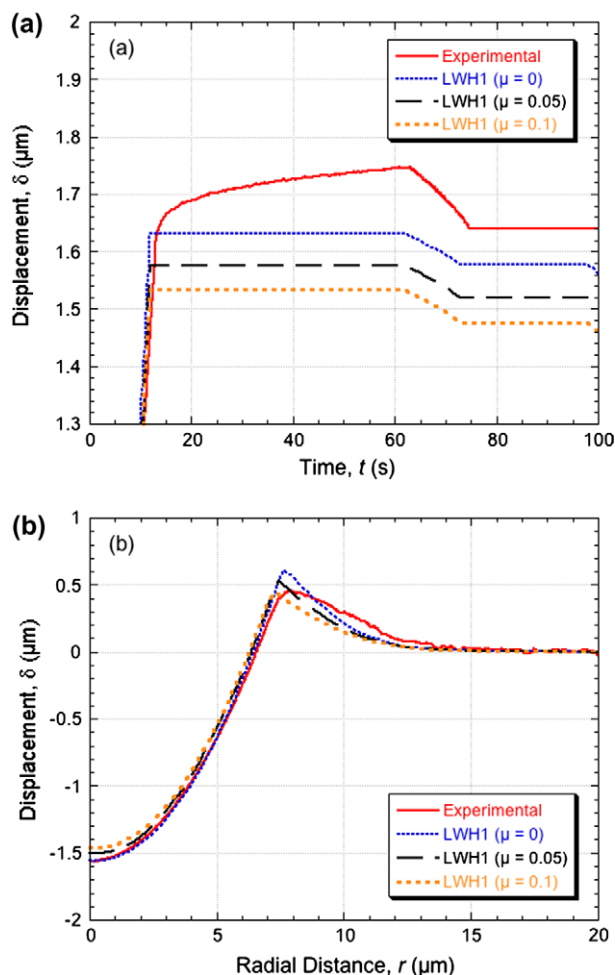


Fig. 9. Comparison, for a loading rate of  $10 \text{ mN s}^{-1}$  (Fig. 6), between experimental data and predictions from the FEM model, obtained using the creep parameters shown in Fig. 5, the LWH1 constitutive relation and the coefficients of friction shown in the legend, for: (a) the displacement history and (b) the residual indent shape.

are created in a region extending about  $10 \mu\text{m}$  below the indenter, with peak stresses of about 200 MPa. This peak stress under maximum load is broadly consistent with the LWH1 constitutive relation, for a strain approaching 100%. However, it is worth emphasizing again that creep is being under-predicted during this modelling. In practice, even for the high loading (and unloading) rate, creep relaxation may reduce the stresses below the levels shown in Fig. 10c, by the time that unloading is complete, and it is certainly clear that they will be appreciably reduced by creep quite soon afterwards.

## 5. Conclusions

The following conclusions can be drawn from this work.

- (a) Quasi-static nanoindentation has been carried out on extruded copper. The data obtained have been compared with predictions from an FEM model, using a range of constitutive relations (one of which corre-

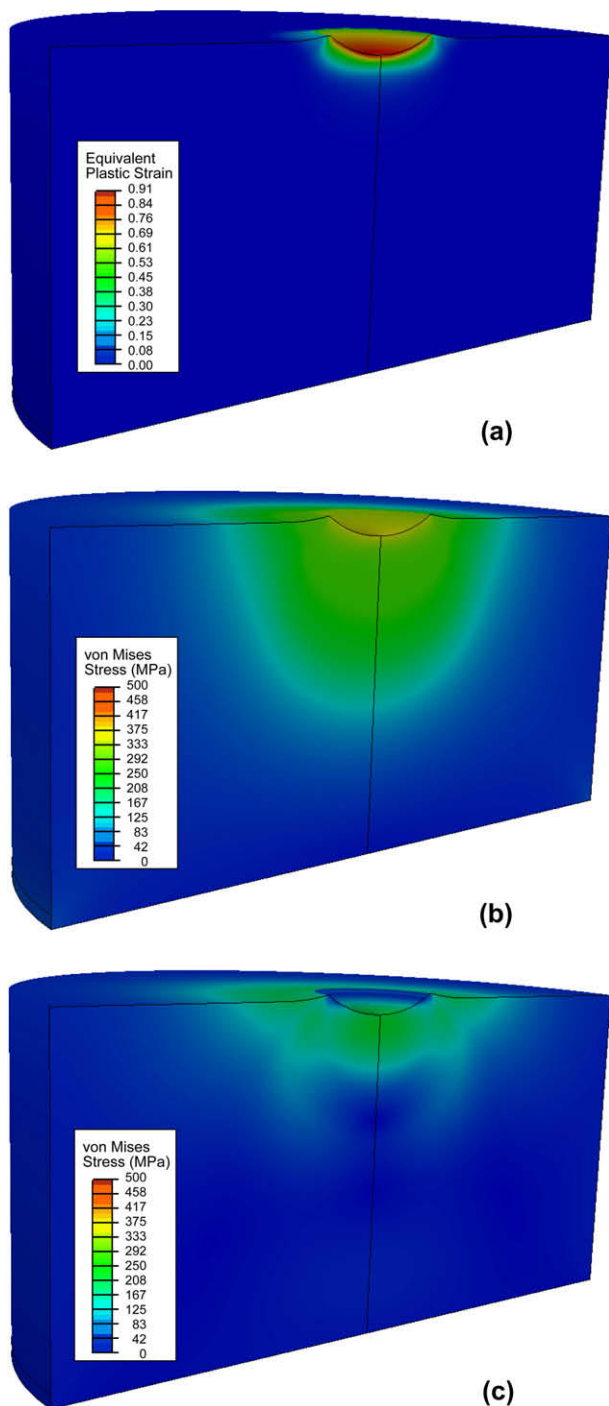


Fig. 10. Predicted fields for the reference case (LWH1, with no friction, the creep parameters shown in Fig. 5 and a loading rate of  $10 \text{ mN s}^{-1}$  (Fig. 6)), showing: (a) residual equivalent plastic strain, (b) von Mises stress at peak indentation depth, and (c) von Mises stress immediately after unloading.

sponded to the macroscopic experimental stress–strain curve) and a fixed set of (steady state) creep parameters (obtained experimentally). The objective was to explore how such comparisons can be optimized, with a view to using them to obtain constitutive relations from nanoindentation data.

- (b) Good agreement was obtained between experimental data and model predictions for the load–displacement–time relationships and for residual indent shapes, using the experimentally obtained constitutive relationship, providing a relatively high loading rate was used, such that creep was not strongly affecting the observed behaviour. The sensitivity to the constitutive relationship in such cases, particularly for the load required to reach a given indenter depth, at a given loading rate, was quite high. On this basis, assuming the correct constitutive relation to be based on a fixed yield stress and a constant work-hardening rate, it would have been possible to establish these values with reasonable accuracy via these comparisons, using the data acquisition and modelling procedures described here. A rough estimate of the probable accuracy with which the yield stress and the work-hardening rate could have been estimated in this way would be  $\pm 10\%$  and  $\pm 25\%$ , respectively. Of course, if it had not been known that the material exhibited linear work-hardening, then the procedure would have been slightly more complex and less accurate.
- (c) For some loading regimes, however, such as when a relatively slow loading rate is employed, the effect of creep deformation is likely to be pronounced, obviously depending on the creep characteristics of the material and the temperature. Even if this creep behaviour were to be relatively well-captured, this would undoubtedly introduce errors into the procedure for deducing the constitutive relation from indentation data. In fact, use of the experimentally obtained (steady state) creep equation in the present work led to a substantial under-prediction of the contribution of creep to the overall deformation. This is probably because primary creep was dominating the observed behaviour, with the associated strain rates being much higher than in the corresponding steady state. In fact, the difference, for the regime of temperature and stress relevant to the indentation testing, was estimated from the creep testing data to be a factor of approximately 100. Of course, the stress level in any particular region tends to change continuously during indentation, inhibiting the establishment of true steady state creep, and there are always regions (peripheral to the plastic strain field) that are entering the primary creep regime. In general, it is clear that considerable attention must be devoted to the possibility that creep deformation is occurring during indentation experiments being used to deduce constitutive relations.
- (d) The predicted effect of friction on the displacement–time response and residual indent shape has been investigated. The data suggest that these responses are expected to show at least some sensitivity to the friction coefficient, over the range in which it is expected to lie, although the best agreement between

experiment and predictions was actually obtained using a value of zero. However, this is a rather tentative conclusion, limited by the accuracy of the experimental data. There is certainly an incentive to measure friction coefficients during indentation, which presents certain experimental challenges.

### Acknowledgements

The authors would like to acknowledge financial support from EPSRC (Platform Grant). There has also been assistance from Mr. Chris Dunleavy, Dr. Sandra Korte and Mr. Robert Stearn, all of the Materials Science Department in Cambridge.

### References

- [1] Fivel M, Verdier M, Canova G. *3D Mater Sci Eng A* 1997;234:923.
- [2] Bouzakis K, Michailidis N, Hadjiyiannis S, Skordaris G, Erkens G. *Zeit Metallk* 2002;93:862.
- [3] Elmustafa A, Stone D. *J Mater Res* 2007;22:2912.
- [4] Bouvier S, Needleman A. *Model Simul Mater Sci Eng* 2006;14:1105.
- [5] Casals O, Ocenasek J, Alcalá J. *Acta Mater* 2007;55:55.
- [6] Chen F, Chang R. *J Mech Sci Technol* 2007;21:1471.
- [7] Guelorget B, Francois M, Liu C, Lu J. *J Mater Res* 2007;22:1512.
- [8] Dao M, Chollacoop N, Van Vliet KJ, Venkatesh TA, Suresh S. *Acta Mater* 2001;49:3899.
- [9] Bouzakis K, Michailidis N. *Thin Solid Films* 2004;469:227.
- [10] Bouzakis K, Michailidis N. *Mater Character* 2006;56:147.
- [11] Lee H, Lee J, Pharr GM. *J Mech Phys Solids* 2005;53:2037.
- [12] Pelletier H. *Tribol Int* 2006;39:593.
- [13] Kim J, Lee K, Lee J. *Surf Coat Technol* 2006;201:4278.
- [14] Lee K, Kim K, Kim J, Kwon D. *J Phys D – Appl Phys* 2008;41:Art. 74014.
- [15] Heinrich C, Waas AM, Wineman AS. *Int J Solids Struct* 2009;46:364.
- [16] Liu Y, Wang B, Yoshino M, Roy S, Lu H, Komanduri R. *J Mech Phys Solids* 2005;53:2718.
- [17] Liu Y, Varghese S, Ma J, Yoshino M, Lu H, Komanduri R. *Int J Plasticity* 2008;24:1990.
- [18] Stelmashenko NA, Walls MG, Brown LM, Milman YV. *Acta Metall Mater* 1993;41:2855.
- [19] Lim YY, Chaudhri MM. *Philos Mag A* 2002;82:2071.
- [20] Mulhearn TO, Tabor D. *J Inst Met* 1960–1961;89:7.
- [21] Mayo MJ, Nix WD. *Acta Metall* 1988;36:2183.
- [22] Bower AF, Fleck NA, Needleman A, Ogbonna N. *Proc Roy Soc Lond A* 1993;441:97.
- [23] Goodall R, Clyne TW. *Acta Mater* 2006;54:5489.
- [24] Chang S, Lee Y, Chang T. *Mater Sci Eng A* 2006;423:52.
- [25] Cavaliere P. *Phys B – Condens Matter* 2008;403:569.
- [26] Tejedor R, Rodriguez-Baracaldo R, Benito J, Caro J, Cabrera J. *Scripta Mater* 2008;59:631.
- [27] Mesarovic SD, Fleck NA. *Proc Roy Soc Lond A* 1999;455:2707.
- [28] Mata M, Alcalá J. *J Mech Phys Solids* 2004;52:145.
- [29] Antunes JM, Menezes LF, Fernandes JV. *Int J Solids Struct* 2007;44:2732.
- [30] Horcas I, Fernandez R, Gomez-Rodriguez JM, Colchero J, Gomez-Herrero J, Baro AM. *Rev Sci Instrum* 2007;78:013705.
- [31] ABAQUS, ABAQUS user manuals, version 6.9; 2009.